Stability analysis of the self-phase-locked divide-by-2 optical parametric oscillator

Petra Groß* and Klaus-Jochen Boller
Department of Applied Physics, University of Twente, 7500 AE Enschede, The Netherlands
(Received 26 July 2004; published 4 March 2005)

The properties of all-optical phase-coherent frequency division by 2, based on a self-phase-locked continuous-wave (cw) optical parametric oscillator (OPO), are investigated theoretically. The coupled field equations of an OPO with intracavity quarter-wave plate are solved analytically in steady-state, yielding a condition for self-phase-locked operation. In the self-phase-locked state, two different values for the pump power at threshold are obtained. By using a linear stability analysis, it is proven that only the lower threshold value is stable, whereas the higher threshold value is unstable. The analytical investigations of the steady-state field values further reveal a twofold symmetry in phase space. The theoretical consideration is completed by a numerical analysis based on the integration of the envelopes of the three OPO fields, which allows for studying the temporal evolution of different initial values. The numerical investigation of the OPO subharmonic phases shows that the two-phase eigenstates are equivalent with respect to experimental parameters and are assumed by the self-phase-locked OPO in dependence of the initial phases of the subharmonic fields, dividing phase space into two symmetric basins of attraction.

DOI: 10.1103/PhysRevA.71.033801 PACS number(s): 42.65.Yj, 42.79.Nv, 42.65.Sf, 42.62.Eh

I. INTRODUCTION

The precise measurement of time via a measurement of optical frequencies is of mayor importance in science and engineering. Modern telecommunication and navigation systems depend on a precise measurement of frequency and the accurate control of corresponding oscillators. Also, the measurement of fundamental physical constants as well as basic research in geophysics or astrophysics are based on techniques involving the precise measurement of optical frequencies.

A prerequisite for the precise measurement of any unknown frequency is the presence of a frequency standard in close vicinity to the frequency to be measured. Today, in the UV, visible and near infrared spectral range optical frequency standards are emerging with a potential precision in the range of 10^{-18} [1]. Especially, the visible and near infrared spectral range from 250 to 750 THz is covered by octave-spanning frequency combs [2]. However, frequency standards lying further in the infrared are scarce, and to measure any frequency in the mid or far infrared, subsequent steps of phase-coherent frequency division are required.

Lately, all-optical self-phase-locked (SPL) optical parametric oscillators (OPOs) have come into interest as phase-coherent frequency dividers [3–5]. These frequency dividers are capable of dividing any frequency and thereby offer the possibility to extend the range accessible for high-precision frequency metrology to the mid and far infrared. However, in order to judge the full potential of such dividers, and for their successful experimental realization, a thorough theoretical understanding of the basic processes of self-phase locking is indispensable.

The current work aims at the theoretical description of an actual experiment, to enable a detailed understanding and a comparison with the experiment. We present an analysis of the steady states and also off-steady-state (dynamical) behavior of an all-optical, self-phase-locked divide-by-2 OPO as sketched in Fig. 1. Recently, Adamyan and Kryuchkyan studied squeezing effects based on a steady-state analysis in a more idealized case (with perfect signal-idler symmetry), and when the pump field is adiabatically eliminated [6]. Our approach follows an earlier theoretical description of such a system by Fabre and colleagues [7]. However, the theoretical description presented in the following sections is carried

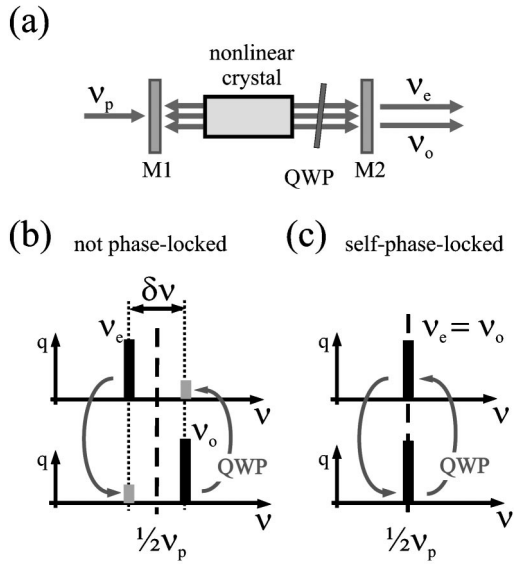

FIG. 1. (a) Schematic setup of an OPO with intracavity quarter-wave plate (QWP) for division of the pump frequency by 2; M1, M2: cavity mirrors, ν_p, ν_e, ν_o: frequencies of the pump, the e- and the o-wave, respectively. (b), (c) Frequency diagram of the self-phase-locking process.

*Electronic address: p.gross@utwente.nl

several steps further. For the first time, a stability analysis is applied to the solutions. The analysis is supported by a numerical evaluation of the coupled field equations, which, unlike the steady-state analysis, enables the study of phase-locking dynamics and the dependence on initial values. In parallel to the theoretical results presented here, we have realized such a divider OPO experimentally. A large measured locking range of 160 MHz with a low fractional frequency instability of better than 5×10^{-14} has been reported [8]. The experimental results have been improved by a direct measurement of the subharmonic phase stability to yield a fractional frequency instability of 8×10^{-18} [9].

This paper is organized as follows. Section II describes the basic concept and working principle of the divide-by-2 OPO. To model the self-phase-locked divide-by-2 OPO, we have started from the coupled wave equations of a triply resonant OPO (Sec. III). The divider's steady-state properties are described analytically in Sec. IV. A stability analysis is applied to the solutions, as described in Sec. V. Finally, Sec. VI introduces the phase eigenstates the OPO can assume in the self-phase-locked regime and reveals a twofold symmetry in phase space. Throughout the paper, the analysis of the self-phase-locked divide-by-2 OPO is supported by a numerical evaluation of the coupled field equations to enable the demonstration of phase-locking dynamics and the dependence on initial values.

II. CONCEPT AND WORKING PRINCIPLE

The basic concept for optical self-phase locking is phase locking of the two OPO subharmonic waves via mutual injection [10]. Here we consider optically self-phase-locked division by 2 in a nearly degenerate type-II OPO, such that the subharmonic waves possess crossed polarizations. For the purpose of mutual injection of these waves, an intracavity quarter-wave plate is used that projects an adjustable fraction of the subharmonic waves onto each other. The schematic setup of the experiment is shown in the upper part (a) of Fig. 1.

The OPO setup we consider here is chosen to enable a straight-forward comparison with ongoing experiments [8,9]. The OPO consists of a nonlinear crystal in a linear two-mirror cavity, which is resonant for the pump wave and for both OPO subharmonic waves (triply resonant). The crystal is birefringent and provides type-II phase matching of the OPO process, so that it converts the ordinary polarized pump wave with frequency ν_p into two subharmonic waves, each with approximately half the pump frequency but with orthogonal linear polarizations. In the further text, we refer to the first subharmonic wave as o-wave, as it possesses ordinary polarization parallel to the pump wave. We will refer to the other subharmonic wave as the e-wave, as it is polarized in the extraordinary direction, perpendicular to the pump and the o-wave. A quarter-wave plate introduces a polarization rotation leading to a mutual injection of the two subharmonic waves into each other.

The diagrams in the lower part of Fig. 1 illustrate the working principle of self-phase locking. Here, the amplitudes of the two subharmonic waves are displayed as a function of frequency. For clarity, the amplitudes of the e- and the o-wave are plotted above each other, on separate axes. Via the quarter-wave plate, a small amount of each wave is transferred (rotated and projected) to the other polarization state, which enables mutual injection. We define the difference between the two light frequencies as $\delta\nu=\nu_e-\nu_o$ [Fig. 1(b)].

If the frequency difference $\delta\nu$ is adjusted by tuning the phase-matching wavelengths and the cavity length of the OPO, such that $\delta\nu$ becomes smaller than a characteristic frequency difference $\delta\nu_{lock}$, i.e., $|\delta\nu|=|\nu_e-\nu_o|\leqslant\delta\nu_{lock}$, one expects injection locking of the e-wave by the o-wave and vice versa.

In contrast to common injection locking of lasers, in the considered OPO-injection locking both waves are generated by the same process, namely optical parametric oscillation. This situation can thus be termed self-injection locking. The e- and the o-wave should then oscillate with the exact frequency ratio of 2:1:1. This situation is depicted in Fig. 1(c), where the e- and the o-wave frequencies equal each other and come to lie at exactly one-half of the pump frequency: $\nu_e=\nu_o=\frac{1}{2}\nu_p$ [see Fig. 1(c)].

In the following section, we introduce a theoretical model that is used to derive the steady-state solutions of such a self-phase-locked divide-by-2 OPO. We will start from the coupled wave equations of an OPO with intracavity quarter-wave plate, and use the support of numerical methods to visualize the effect of phase locking.

III. THEORETICAL MODELING

A. Coupled field equations

The nonlinear wave mixing processes in the OPO can be described, in the mean-field, plane-wave approximation, by three coupled equations for the OPO internal electric field $q(t)=q_p(t)e^{i\Omega_p t}+q_e(t)e^{i\Omega_e t}+q_o(t)e^{i\Omega_o t}$. The carrier frequencies Ω_p, Ω_e, and Ω_o are chosen to be the frequencies of an exact divider, i.e., $\Omega_e=\Omega_o=\Omega_p/2$. If the OPO frequencies are close to these carrier frequencies, the complex amplitudes q_p, q_e, and q_o are slowly varying with time. In case that the amplitude variations are of oscillatory nature, their oscillation frequencies are the frequency deviations of the OPO fields from the frequencies that correspond to an exact division by 2. We choose $\Omega_p\equiv2\pi\nu_p$, where ν_p is the given frequency of an external pump laser driving the OPO, such that also the carrier frequencies Ω_e and Ω_o are determined by the pump laser frequency. The coupled equations for the intracavity field amplitudes can then be written as follows [11]:

$$\frac{d}{dt}q_p=-\frac{1}{2}\kappa_p q_p+iDq_e q_o+F, \tag{1a}$$

$$\frac{d}{dt}q_e=-\frac{1}{2}(\kappa_e-i\Delta_e)q_e+iDq_o^* q_p+\gamma q_o, \tag{1b}$$

$$\frac{d}{dt}q_o=-\frac{1}{2}(\kappa_o-i\Delta_o)q_o+iDq_p q_e^*-\gamma^* q_e. \tag{1c}$$

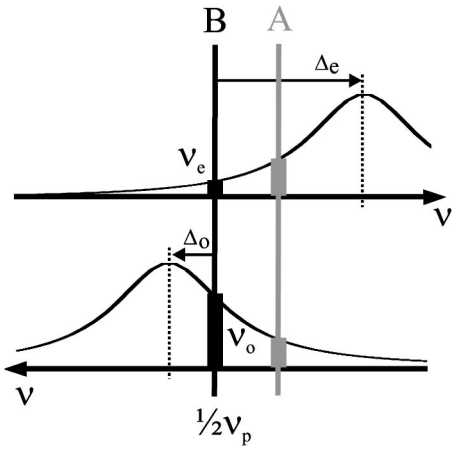

FIG. 2. Definition of the cavity detunings Δ_e and Δ_o of the phase-locked OPO. The line shape of the cavity modes and the light frequencies of the e-wave (upper axis) and of the o-wave (lower axis) are plotted as a function of frequency: from left to right, the e-wave frequency increases, while the o-wave frequency decreases. The cavity detunings Δ_e and Δ_o are given by the distances between half the pump frequency and the nearest cavity modes.

This approach follows the earlier investigation of such a system by Fabre and colleagues [7] and our study of a divide-by-3 OPO, where similar coupled field equations were introduced to describe self-phase-locked frequency-by-3 division [3].

The field amplitudes q_x are normalized such that the squares of their absolute values give the intracavity photon numbers $N_x=|q_x|^2$ [11], where the indices $x=p,e,o$ designate the pump wave, the e- and the o-wave, respectively.

The first terms on the right-hand side (RHS) of Eqs. (1a)–(1c) describe the decay of the field amplitudes due to resonator losses, with the cavity decay rates κ_x.

The last term in Eq. (1a), F, describes the pumping of the OPO with the external laser that is to be frequency divided. F is a field pump rate, which is proportional to the square root of the pump laser power P_p times the pump input transmission of the cavity mirror M1.

The terms containing the nonlinear coupling coefficient D give the strength of nonlinear interaction of the pump wave, the e-, and the o-wave. The value of D depends on construction parameters of the OPO and the involved light frequencies.

The values of Δ_e and Δ_o give the detunings of the OPO's cold cavity modes from exact division by 2. Note that, in an experiment, the detunings can be changed via changing the optical cavity length. Further, we assumed a zero detuning of the pump cavity from the pump frequency, i.e., $\Delta_p=0$. This assumption is well-justified, because usually for continuous operation of a triply resonant OPO, the pump cavity length is electronically locked to the pump laser wavelength. In the theoretical model, we consider only subharmonic oscillation in those cavity modes that are closest to frequency degeneracy, which experimentally can be guaranteed due to an appropriate tuning strategy.

To better illustrate the definition of the cavity detunings, they are depicted schematically in Fig. 2. The cold cavity modes are shown as Lorentzian-like curves as a function of frequency. For later convenience, the e-wave frequency axis is chosen such that the frequency increases to the right (upper part), while the o-wave frequency increases to the left (lower part). Due to the crystal's birefringence, the optical resonator length and thus also the detuning of the cold cavity modes from exact division by 2 are different for the e-wave and the o-wave. Further, the two axes are positioned relative to each other such that at any arbitrary vertical line the sum of the two frequencies found at the intersection points gives the pump frequency. Thus, any two optical frequencies that can be generated by the OPO need to lie precisely above each other in order to fulfill energy conservation $\nu_e+\nu_o=\nu_p$ (see, e.g., line A). In self-injection-locked (or self-phase-locked) oscillation, however, the e-wave and the o-wave frequencies assume the identical value (see line B) and are thus locked to exactly half of the pump frequency.

Note, that the non-phase-locked (free-running) operation of the OPO is a completely different mode of oscillation, and one has to clearly distinguish between that state and the phase-locked state. In the free-running case, the OPO will adjust its frequencies to minimize the cavity losses, such as for line A in Fig. 2 [11].

The last terms on the RHS of Eqs. (1b) and (1c) describe the mutual injection of the two OPO subharmonic fields introduced by the intracavity quarter-wave plate. The parameter γ is a measure for the injection (coupling) strength and increases with the experimentally adjustable angle of the QWP's fast axis (see Sec. III B).

B. Parameters used for the evaluation

For an analytical and numerical investigation, we follow the approach of Fabre *et al.* [7] and separate the complex field amplitudes q_x into real positive amplitudes b_x and real phases φ_x by setting $q_x=b_x e^{i\varphi_x}$. The same way, the pump rate F is separated into a real, positive amplitude f and a real phase β, $F=fe^{i\beta}$, as well as the complex coupling parameter γ, $\gamma=\gamma_0 e^{i\theta}$. The coupling strength is proportional to the part of the e-wave and the o-wave, which is transferred to the other polarization state, and is given by [7]

$$\gamma=\sin(2\vartheta_{QWP})\sqrt{\kappa_e\kappa_o}e^{i\theta}, \tag{2}$$

in which ϑ_{QWP} is the rotation angle of the QWP. The factor 2 occurs because in the considered standing-wave cavity the QWP is passed twice per round trip. The phase θ takes into account a propagational phase shift that the waves acquire while traveling through the quarter-wave plate.

With the described notation the coupled field equations (1a)–(1c) can be separated into six equations that describe the temporal changes of the real amplitudes b_x and the real phases φ_x of the OPO fields.

These not explicitly shown expressions for $(d/dt)b_x$ and $(d/dt)\varphi_x$ are the basis for the numerical integration of the coupled field equations, which is introduced in the subsequent Sec. III C, and are used to analytically derive the steady-state solutions of the self-phase-locked divide-by-2 OPO in Sec. IV.

TABLE I. Parameters for the cavity losses and the nonlinear coupling coefficient as used for the calculations.

κ_p	κ_e	κ_o	D
336 MHz	114 MHz	117 MHz	1050 Hz

In summary, studying the dynamical behavior of the OPO with self-injection locking comprises of finding the time dependence of six variables $Q=\{b_p, b_e, b_o, \varphi_p, \varphi_e, \varphi_o\}$, taking into account a set of ten external parameters $P=\{\kappa_p, \kappa_e, \kappa_o, \Delta_e, \Delta_o, f, \beta, \gamma_0, \theta, D\}$. The variables can either be calculated by numerical integration (starting with some initial values $Q^{(0)}=\{b_p^{(0)}, b_e^{(0)}, b_o^{(0)}, \varphi_p^{(0)}, \varphi_e^{(0)}, \varphi_o^{(0)}\}$), such as shown in Sec. III C. The steady-state values can also be calculated analytically, as is described in Sec. IV. For both calculations we assume that a part of the external parameters is constant, which are the cavity losses κ_p, κ_e, and κ_o and the nonlinear coupling coefficient D. The values used for this work are determined from our actual experimental setup and are summarized in Table I (their derivation is analogous to the description in Ref. [12]). The remaining experimental parameters are not constant but can be slowly varied during operation of the OPO, such as the detunings Δ_e and Δ_o (via changing the cavity length), the pump parameters f and β (via the pump laser), and the self-injection parameters γ_0 and θ (via a rotation of the QWP).

It shows that, depending on the choice and variation of the latter parameters, the behavior of the system falls in one of two different regimes. First, there is a regime where the parameter choice leads to operation of the OPO in a non-phase-locked or *free-running* regime. In this case, the solutions for the field envelopes in Eqs. (1a)–(1c) will show some oscillatory behavior. In this case, the total electric field, $A_{e,o}(t)=q_{e,o}(t)e^{2\pi i(\nu_p/2)t}$, contains optical side bands, indicating that the phases of the OPO subharmonic waves change with respect to each other and the pump wave.

In the second regime, by choosing the external system parameters to lie within a certain range, the solutions of Eqs. (1a)–(1c) will become time independent, constant field amplitudes. The subharmonic OPO light fields then attain the form $A_{e,o}(t)=A_{e,o}^0 e^{2\pi i(\nu_p/2)t+\varphi_{e,o}^0}$. In this case, the e- and the o-waves will be oscillating with constant relative phases or *phase-locked*, and the OPO works as a phase-coherent frequency divider.

C. Numerical evaluation

To illustrate the dynamical behavior in these two distinct regimes we present here two typical examples of the temporal evolution of the OPO fields.

For this purpose we numerically integrate the coupled field equations using a fourth-order Runge-Kutta method [13] with small initial values for the e- and o-field amplitudes.

For the first example, shown in Fig. 3, we used (fixed) external parameters of our experimental setup (see Table I). As the variable external parameters we used a quarter-wave plate rotation angle of $\vartheta_{QWP}=6°$, and a pump rate of $f=1.22\times10^{13}$ Hz (corresponding to an external pump power of 300 mW). Further we used cavity detunings of $\Delta_e=+32$ MHz and $\Delta_o=+8$ MHz, i.e., the e- and o-wave cavities are detuned by rather different values.

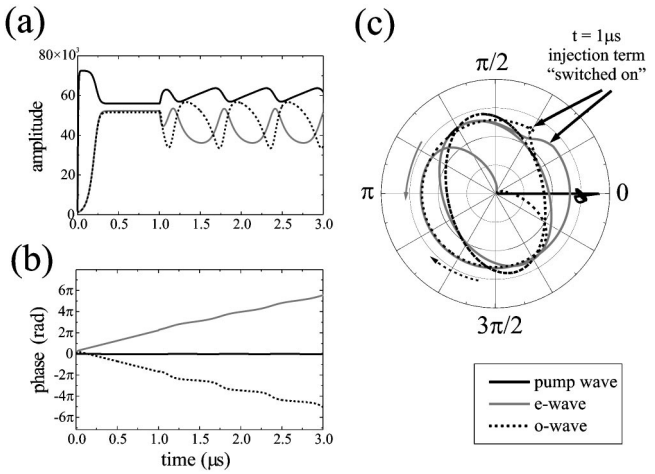

FIG. 3. Time evolution of (a) the amplitudes and (b) the phases of the OPO fields for cavity detunings of $\Delta_e=32$ MHz and $\Delta_o=8$ MHz. (c) Results summarized in a polar coordinate system with amplitudes as radius and phases as angle. Solid black curve: pump wave; solid gray curve: e-wave; dashed black curve: o-wave.

Figure 3(a) shows the resulting amplitudes, and Fig. 3(b) the phases of the resonator-internal pump wave, the e-wave and the o-wave as a function of time. The pump wave data are displayed as a solid black curve, the e-wave as a solid gray curve and the o-wave as the dashed black curve. For a better illustration of the effect of mutual injection of the e- and the o-wave, the self-injection terms are only after some delay of 1 μs [i.e., $\gamma=0$ in Eqs. (1a)–(1c) for $t<1$ μs] turned to a constant value which, in the case of Fig. 3, is $\gamma_0=\sin(2\times6°)\sqrt{\kappa_e\kappa_o}=0.21\sqrt{\kappa_e\kappa_o}$.

It can be seen that, upon turn-on of the pump term at $t=0$ the intracavity pump field rises, followed by an onset of parametric oscillation. After about 0.5 μs, all amplitudes reach steady state. However, the phases of the e- and the o-wave maintain to diverge linearly as a function of time, with equal slope of opposite sign. The absolute values of the slopes correspond to the sum of the chosen cavity detunings, which is 40 MHz in our example. The opposite sign of the diverging phases shows that the sum of the e- and the o-phases remains constant with respect to the resonator-internal pump phase, which is one of the main characteristics of OPOs [14]. Note that the resonator-internal pump phase is displayed with respect to the phase of the external pump laser field, and that the internal phase follows the external phase with only small deviations.

From Fig. 3(a) for $t>1$ μs one can see that after the injection coupling term is "switched on," the formerly steady subharmonic amplitudes start oscillating. At the same time, their phases continue to diverge, with only a weak oscillation superimposed.

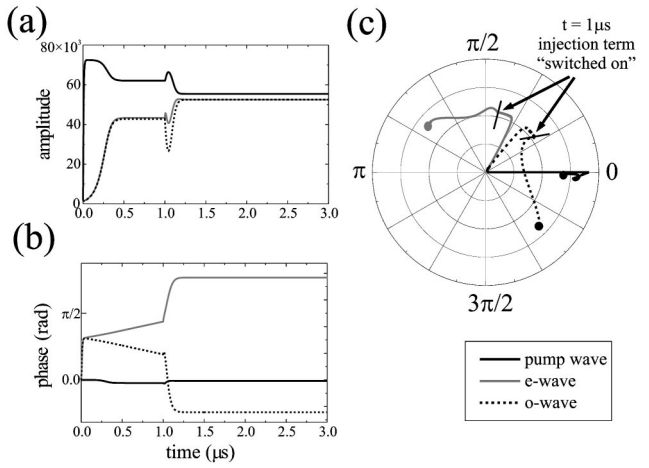

FIG. 4. Time evolution of (a) the amplitudes and (b) the phases of the OPO fields for cavity detunings of $\Delta_e=\Delta_o=60$ MHz. In (c) the results are plotted together in a polar coordinate system with amplitudes as radius and phases as angle. Solid black curve: pump wave; solid gray curve: e-wave; dashed black curve: o-wave.

The temporal dynamics of graphs 3(a) and 3(b) are summarized in Fig. 3(c) as a polar diagram. Here the complex amplitude of the three fields is displayed as radius and a corresponding phase angle, which results in three traces in Fig. 3(c). Upon startup of the OPO, the pump trace, the e-, and the o-wave traces emerge out of the origin. Thereafter, the e- and the o-wave fields rotate about the origin, initially on a circle with a constant angular velocity given by the sum of the chosen cavity detunings. Turning on the self-injection terms (see the arrows pointing to $t=1$ μs) alters the circular traces into traces resembling an *elliptic* shape. The direction of the e- and o-rotation is maintained, as well as their average angular velocity given by the number of revolutions per time.

From the continuing divergence of the e- and o-waves' phases displayed in Fig. 3(b), one can clearly see that a phase locking does not occur, in spite of a mutual injection locking. The main consequence of our particular choice of parameters is an oscillation. The latter modulation indicates that the mutual e- and o-wave injection gives rise to optical side bands on the pump, the e- and the o-field.

As a second example, we consider an OPO with the identical parameters as before, but now we choose symmetrical cavity detunings of $\Delta_e=\Delta_o=60$ MHz. The results of the numerical integration are shown in Fig. 4.

Again, the amplitudes reach a steady state after about 0.5 μs [Fig. 4(a)], while the phases diverge continuously [Fig. 4(b)], now with a rate of 2×60 MHz 2π. However, after the injection terms are activated at 1 μs, the divergence of the phases is first accelerated before the phase divergence stops. Attaining constant e- and o-wave phases takes about 0.25 μs. Thereafter the e- and o-fields oscillate in phase with the pump field, which is a clear evidence of self-phase locking. Note that also the pump phase inside the OPO cavity, which has been adjusted to −73 mrad with respect to the external pump phase for the case of the free running OPO

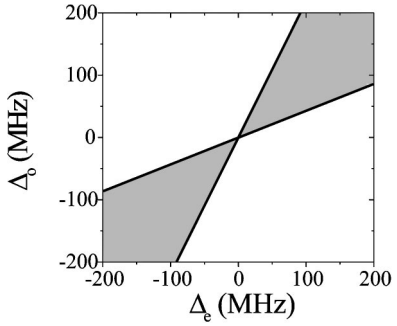

FIG. 5. Parameter plane spanned by the cavity detunings. The gray area gives the theoretically calculated sets of cavity detunings (Δ_e,Δ_o), for which the OPO is self-phase-locked. The locking area is calculated with the experimental parameters κ_e and κ_o and with a QWP angle of 6°.

(i.e., before the injection terms are activated), now is adjusted to a slightly different value, namely to −24 mrad. One can see in Fig. 4(a) that, upon self-injection locking, also the absolute field amplitudes attain new values. Specifically, the amplitudes of the e- and o-waves are significantly higher than without self-phase locking in the free-running steady-state OPO. The latter indicates that self-phase locking lowers the pump power at threshold.

In summary, the presented examples of numerical integration have shown that mutual self-injection of the OPO subharmonic waves can lead to self-phase locking and phase-coherent frequency division, accompanied by a lower threshold and increased output, but that this strongly depends on the parameters of operation, such as the cavity detunings.

IV. STEADY-STATE SOLUTION

A. Locking condition

To generalize the findings from the numerical integration, the coupled field equations are solved analytically in the steady-state regime. The goal is to find the conditions for self-phase-locked oscillation and to derive corresponding expressions for the phase eigenstates of the locked fields.

As a first step, we consider the two coupled field equations (1b) and (1c) applying steady-state conditions, i.e., zero time derivatives on the LHS. One then obtains four linear coupled equations for q_e and q_o, and for their complex conjugates q_e^* and q_o^*, which can be expressed in matrix form:

$$\frac{d}{dt}\begin{pmatrix} q_e \\ q_o \\ q_e^* \\ q_o^* \end{pmatrix} = 0 = \mathbf{A} \times \begin{pmatrix} q_e \\ q_o \\ q_e^* \\ q_o^* \end{pmatrix} \tag{3}$$

with the 4×4 matrix

$$\mathbf{A} = \begin{pmatrix} -\frac{1}{2}(\kappa_e - i\Delta_e) & \gamma & 0 & iDq_p \\ -\gamma^* & -\frac{1}{2}(\kappa_o - i\Delta_o) & iDq_p & 0 \\ 0 & -iDq_p^* & -\frac{1}{2}(\kappa_e + i\Delta_e) & \gamma^* \\ -iDq_p^* & 0 & -\gamma & -\frac{1}{2}(\kappa_o + i\Delta_o) \end{pmatrix}. \tag{4}$$

This equation has nonzero electric field solutions only if the determinant of **A** is zero. With the separation of the complex field amplitudes b_x, the pump rate F, and the coupling coefficient γ into real amplitudes and phases, the determinant is calculated to yield the following expression:

$$D^2 b_p^2 = \gamma_0^2 + \frac{1}{4}\kappa_e\kappa_o + \frac{1}{4}\Delta_e\Delta_o \pm \frac{1}{4}\sqrt{\alpha}, \tag{5}$$

where the abbreviation α is defined as

$$\alpha = 16\gamma_0^2\Delta_e\Delta_o - (\Delta_e\kappa_o - \Delta_o\kappa_e)^2. \tag{6}$$

Except for the expression for α, all terms of Eq. (5) are real; the term b_p^2 on the LHS of the equation is even a directly measurable quantity, as it is equal to the intracavity pump photon number. Therefore the complete RHS of Eq. (5) must be real, which means that $\sqrt{\alpha}$ must be real as well. From $\alpha(\Delta_e,\Delta_o) \geqslant 0$ one obtains the following condition for an OPO operating in a steady self-injection-locked state:

$$16\gamma_0^2\Delta_e\Delta_o \geqslant (\Delta_e\kappa_o - \Delta_o\kappa_e)^2. \tag{7}$$

Note that if the QWP is set to a neutral position ($\vartheta_{QWP}=0$), such that $\gamma_0=0$, condition (7) reduces to $\Delta_e\kappa_o-\Delta_o\kappa_e=0$, which is the standard condition for unlocked, free-running OPO operation [11].

In contrast to this, for a nonzero quarter-wave plate rotation angle, locking can occur only for those pairs of cavity detunings, Δ_e and Δ_o, which satisfy Eq. (7), such that α in Eq. (6) is real and positive. For example, using the specific experimental parameters $\kappa_e=114$ MHz and $\kappa_o=117$ MHz of the OPO that are present in our experiments (compare Table I in Sec. III B), and assuming a QWP angle $\vartheta_{QWP}=6°$, which is the largest angle that could be realized experimentally, we obtain from Eq. (7) that locking can occur if the ratio of the detunings, Δ_e/Δ_o, lies between 0.43 and 2.19.

This range of locked steady-state operation is depicted schematically in Fig. 5, in a plane spanned by the cavity detunings. Locking can occur only for detunings Δ_e and Δ_o that fall into the gray area bound by the two lines $\Delta_e/\Delta_o=0.43$ and $\Delta_e/\Delta_o=2.19$. It is thus appropriate to speak of a locking area rather than a locking range. According to Eq. (7), the angle between the two diagonals widens with increasing coupling strength γ_0 and thus with increasing quarter-wave plate rotation angle ϑ_{QWP}. Note, however, that the diagonals approach the horizontal or vertical axis only asymptotically and that there is no locking observable for any QWP angle, if the OPO is operated with detunings of opposite sign, $\Delta_e\Delta_o<0$.

B. Intracavity pump photon number

Besides the locking condition of Eq. (7), the solution of the determinant of Eq. (3) also yields information about the intracavity pump field, b_p, and the pump photon number, $N_p=b_p^2$, once the cavity detunings are given [see Eqs. (5) and (6)]:

$$N_{p,\pm} = b_{p,\pm}^2 = \frac{1}{D^2}\left(\gamma_0^2 + \frac{1}{4}\kappa_e\kappa_o + \frac{1}{4}\Delta_e\Delta_o \pm \sqrt{\alpha}\right). \tag{8}$$

From Eq. (8), one finds, independent of the external pump rate F, two different solutions for the intracavity pump field b_p, because of the two possible signs of $\sqrt{\alpha}$. As, above threshold, the intracavity pump photon number N_p is clamped to its threshold value [15], these two solutions belong to two different pump powers at threshold $N_{th,\pm}=N_{p,\pm}=b_{p,\pm}^2$. Here and in Eq. (8), the upper of the signs $\pm$ designates the high-threshold solution $b_{p,+}$, and the lower one the low-threshold solution, $b_{p,-}$. According to Eq. (6), the difference between the two threshold values increases with increasing γ_0 symmetrically about the free-running threshold and is a function of the detunings Δ_e and Δ_o. In particular this means that with increasing rotation angle of the intracavity QWP, the lower threshold of the locked OPO can be brought considerably below the threshold of the free-running OPO.

The described threshold splitting was first predicted by Fabre and colleagues [7], inspired by Mason's experiment [5], where a divide-by-two OPO with an intracavity quarter-wave plate showed two different polarization states. As one polarization state has been observed more often than the other, this was taken as evidence of the OPO operating preferably in the lower-threshold state. However, we claim that their addressing of the two polarization states to the two threshold states is not possible, but that their findings rather show that there exist two distinct phase states for each threshold state. This will be proven in detail via a stability analysis in Sec. V.

Finally, in order to complete the information of the shape of the dividers locking area, one has to consider that any divider is pumped with a finite pump power. This means that increasing the product of the detunings, $\Delta_e\Delta_o$ in Eq. (5), increases the intracavity pump photon number $N_p=b_p^2$, which corresponds to a rising threshold pump power. If $\Delta_e\Delta_o$ is chosen too large, such that N_p exceeds the value that can be provided by the external pump laser, the OPO will not oscillate even if, formally, the detunings fulfill the locking condition of Eq. (7). The resulting restriction of the area of locked oscillation is depicted in Fig. 6, for both the low-threshold

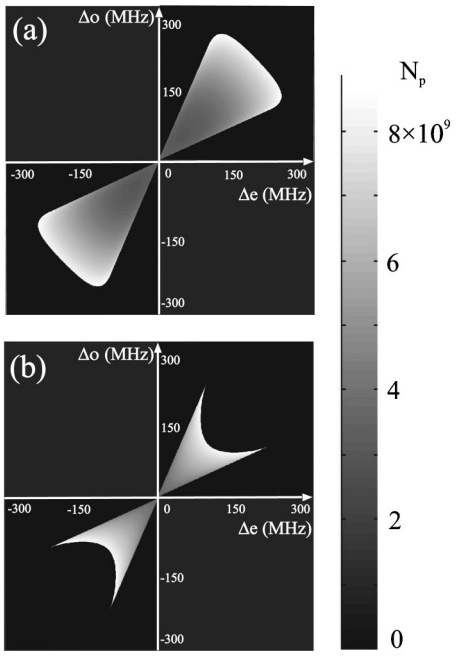

FIG. 6. Intracavity pump photon number (a) for the lower pump power threshold value and (b) for the higher value as two-parameter plots of the cavity detunings Δ_e and Δ_o, calculated with a QWP angle of $\vartheta_{QWP}=6°$. The intracavity pump photon numbers are coded using gray scales.

case (a), and for the high-threshold case (b). The locking area is shown calculated for a particular combination of the QWP angle and pump power (6° and 300 mW, respectively), but analogue calculations show that increasing the pump power increases the extension of both locking areas radially. Increasing the QWP angle leads to an angular widening of both areas (a) and (b), and to a radial increase in (a) and a radial decrease in (b).

C. Phase states and output wave powers

Of special interest are the steady-state values of the subharmonic waves' phases (phase eigenvalues) and their dependence on the external OPO parameters (such as Δ_e, Δ_o, or the phase of the external pump wave, because this determines the phase and frequency fidelity of the divide-by-2 OPO. In this section, we derive the divider's phase eigenstates via the photon numbers of the subharmonic waves.

Using linear combination of the coupled field Eqs. (1a)–(1c) in steady state, i.e., $(d/dt)b_x=0$, $(d/dt)\varphi_x=0$, we obtain expressions containing the sum and difference phases:

$$\sin(\varphi_e+\varphi_o-\varphi_p)=\frac{1}{4Db_p}\left(\kappa_e\sqrt{\frac{\Delta_o}{\Delta_e}}+\kappa_o\sqrt{\frac{\Delta_e}{\Delta_o}}\right), \quad (9)$$

$$\cos(\varphi_e-\varphi_o-\theta)=\pm\frac{1}{4\gamma_0}\left(\kappa_e\sqrt{\frac{\Delta_o}{\Delta_e}}-\kappa_o\sqrt{\frac{\Delta_e}{\Delta_o}}\right), \quad (10)$$

where the $\pm$ sign in Eq. (10) depends on the sign of the detunings Δ_e and Δ_o.

Equations (9) and (10) show that, for a given set of experimental parameters, the phases of the OPO subharmonic fields assume fixed values with respect to the phase of the cavity internal pump field, φ_p. Below we will also derive an expression for the cavity internal pump phase with respect to the external pump phase.

Note that, for the free-running OPO ($\vartheta_{QWP}=0°$ and hence $\gamma_0=0$), only the sum of the subharmonic phases $\varphi_e+\varphi_o$ assumes a defined value, $\overline{(\varphi_e+\varphi_o)}$, which follows the pump phase according to Eq. (9). In contrast, the difference phase $(\varphi_e-\varphi_o)$ is to change versus time [14], such that the individual subharmonic phases undergo a synchronized phase-diffusion process.

Only if the OPO is self-phase-locked through choosing a nonzero QWP rotation angle, the phase-diffusion process is suppressed. Actually, the phase difference is locked to a constant value given by Eq. (10). In this case the phases of the e- and the o-wave assume the constant values φ_e and φ_o.

On closer inspection of Eqs. (9) and (10), where the phase arguments on the LHS are defined only modulo 2π, we find that the subharmonic phases can assume one of two possible values, namely $(\varphi_{e,1},\varphi_{o,1})$ or $(\varphi_{e,2},\varphi_{o,2})=(\varphi_{e,1}+\pi,\varphi_{o,1}+\pi)$. The existence of two-phase eigenstates for a divide-by-2 OPO agrees with an earlier prediction, according to which an all-optical divider by n should possess n phase eigenstates [16].

Using linear combination of Eqs. (1a)–(1c), one can derive the intracavity photon numbers of the e- and the o-wave:

$$N_e=b_e^2=\frac{4fb_p\cos(\varphi_p-\beta)-2\kappa_p b_p^2}{\kappa_e+\kappa_o\dfrac{\Delta_e}{\Delta_o}}, \quad (11)$$

$$N_o=b_o^2=\frac{4fb_p\cos(\varphi_p-\beta)-2\kappa_p b_p^2}{\kappa_o+\kappa_e\dfrac{\Delta_o}{\Delta_e}}. \quad (12)$$

Per roundtrip, a certain percentage of the photons is coupled out through the cavity mirror; therefore the output power of the according wave is a proportional measure of the intracavity photon number.

Finally, the phase of the cavity internal pump field, φ_p, can be determined to be

$$\cos(\varphi_p-\beta)=\frac{1}{f\kappa_p b_p}\left[f^2+\frac{1}{4}\kappa_p^2 b_p^2-\left(\sqrt{f^2-\frac{1}{4}\kappa_p^2 b_p^2(1-\sin^2(\varphi_e+\varphi_o-\varphi_p))}+\frac{1}{2}\kappa_p b_p\sin(\varphi_e+\varphi_o-\varphi_p)\right)^2\right], \quad (13)$$

where $\sin(\varphi_e+\varphi_o-\varphi_p)$ is given by Eq. (9).

Summarizing this section, analytical expressions for the amplitudes and phases of the coupled fields of the self-phase-locked OPO have been derived. With these expressions, the set of variables $\overline{Q}=\{\overline{b_p},\overline{b_e},\overline{b_o},\overline{\varphi_p},\overline{\varphi_e},\overline{\varphi_o}\}$ assumed by the divide-by-2 OPO in steady state can be determined from the experimental parameters. In the self-phase-locked state, we obtained two different values for the pump power at thresh-

old, and for each of the two threshold states, two possible sets of subharmonic phases are revealed.

From the considerations of this section, the question arises what one could expect to measure in the experiment. Is it possible to observe two distinct pump powers at threshold as suggested by Eq. (8) and reported by Mason [5]? And further, would there be phase states observable, two for either one of the two threshold states? What would be the stability of these phase states with respect to small phase perturbations? These questions are of elemental importance to predict the behavior of the frequency divider regarding its suitability for high precision metrology. If the self-phase-locked OPO reacted to external disturbances, e.g., by hopping from one stable state to another one, this would limit its use as a frequency divider.

V. LINEAR STABILITY ANALYSIS

A. Triply resonant case

To determine which of the above derived possible steady-state solutions are stable, a linear stability analysis is applied to the nonlinear dynamical system described by Eqs. (1a)–(1c). A similar stability analysis has been applied by Zondy and colleagues to the steady-state solutions of a divide-by-3 OPO, which also reveals two threshold states. In the case of a doubly resonant divide-by-3 OPO, where both subharmonic waves are enhanced in a resonator, the low-threshold state was found to be stable, while the high-threshold state was found to be unstable [17]. In the case of a pump-enhanced, singly resonant divide-by-3 OPO, on the other hand, both states have been found to be stable [18].

To study the stability of an equilibrium point of the 6-dimensional nonlinear system, we perform a linear approximation of the temporal evaluation of the complex field amplitudes q_p, q_e, q_o and their complex conjugates q_p^*, q_e^*, and q_o^*, which are implicitly contained in Eqs. (1a)–(1c). According to Poincaré, the characteristics of a system's stability can be determined by performing a stability analysis to such a linearized system (with one exception, namely a center, for which the higher order terms become decisive) [19,20]. The linear approximation is obtained by expressing these six equations as Taylor series in the neighborhood of the singular point $\underline{Q}=\{\overline{q_p},\overline{q_e},\overline{q_o},\overline{q_p^*},\overline{q_e^*},\overline{q_o^*}\}$ and neglecting second- and higher-order terms. We define $q_x(t)=\overline{q_x}+\Delta q_x(t)$ and $q_x^*(t)=\overline{q_x^*}+\Delta q_x^*(t)$, where $\overline{q_x}$ and $\overline{q_x^*}$ are the steady-state values, and where the small fluctuations are expressed by $\Delta q_x=\Sigma_\lambda e^{\lambda t}\delta q_x$ and $\Delta q_x^*=\Sigma_\lambda e^{\lambda t}\delta q_{\underline{x}}^*$.

The linearization around Q yields an equation of motion for the fluctuations depending on the eigenvalues λ:

$$\sum_\lambda \lambda e^{\lambda t}\begin{pmatrix}\delta q_p\\ \delta q_e\\ \delta q_o\\ \delta q_p^*\\ \delta q_e^*\\ \delta q_o^*\end{pmatrix}=\mathbf{A}\cdot\sum_\lambda e^{\lambda t}\begin{pmatrix}\delta q_p\\ \delta q_e\\ \delta q_o\\ \delta q_p^*\\ \delta q_e^*\\ \delta q_o^*\end{pmatrix}, \tag{14}$$

with **A** being a linear matrix.

The eigenvalues of the system are found by calculating the determinant of $\mathbf{A}-\lambda\cdot\mathbf{I}$, where **I** is the unity matrix. For the self-phase-locked divide-by-2 OPO described by Eqs. (1a)–(1c) this determinant reads

$$\begin{vmatrix}
-\frac{1}{2}\kappa_p-\lambda & iD\overline{q_o} & iD\overline{q_e} & 0 & 0 & 0\\
iD\overline{q_o^*} & -\frac{1}{2}(\kappa_e-i\Delta_e)-\lambda & \gamma & 0 & 0 & iD\overline{q_p}\\
iD\overline{q_e^*} & -\gamma^* & -\frac{1}{2}(\kappa_o-i\Delta_o)-\lambda & 0 & iD\overline{q_p} & 0\\
0 & 0 & 0 & -\frac{1}{2}\kappa_p-\lambda & -iD\overline{q_o^*} & -iD\overline{q_e^*}\\
0 & 0 & -iD\overline{q_p^*} & -iD\overline{q_o} & -\frac{1}{2}(\kappa_e+i\Delta_e)-\lambda & \gamma^*\\
0 & -iD\overline{q_p^*} & 0 & -iD\overline{q_e} & -\gamma & -\frac{1}{2}(\kappa_o+i\Delta_o)-\lambda
\end{vmatrix}=0. \tag{15}$$

The eigenvalues λ are the solutions of the sixth-order characteristic equation (15), which can be abbreviated as

$$\lambda^6+\xi_5\lambda^5+\xi_4\lambda^4+\xi_3\lambda^3+\xi_2\lambda^2+\xi_1\lambda+\xi_0=0, \tag{16}$$

where all five coefficients are real. The explicit form of the coefficients ξ_k with k ranging from 5 to 0 is given in Appendix A.

It shows that the coefficients are functions of the OPO's construction parameters κ_p, κ_e, κ_o, Δ_e, Δ_o, D, and γ_0, but also of the steady-state solutions b_p, b_e, b_o, φ_p, φ_e, and φ_o, and thus of the pump rate f and the pump phase β. Note that as the steady-state values are different for the low- and the high-threshold solution, this leads to two different characteristic equations for these cases. However, the coefficients and hence the characteristic equation remain the same for both phase eigenstates belonging to the same threshold state. The subharmonic phases enter the coefficients only via $\sin(\varphi_e-\varphi_o-\theta)$ [compare Eqs. (A5), (A7), and (A10)], which attains the same value for both eigenstates.

To illustrate relevant examples of stability, the eigenvalues have been calculated for the experimental parameters summarized in Table I for the cavity detunings $\Delta_e=50$ MHz and $\Delta_o=45$ MHz, for a quarter-wave plate rotation

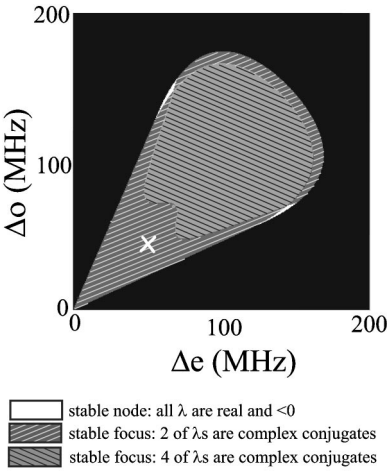

FIG. 7. Different kinds of equilibria calculated for the low-threshold solution with a quarter-wave plate angle of 6° and a pump rate of 1.22×10^{13} Hz, displayed as a function of the cavity detunings Δ_e and Δ_o. The low-threshold solutions are always found to be stable.

angle of $\vartheta_{QWP}=6°$, and for a pump rate of $f=1.22\times10^{13}$ Hz, corresponding to an external pump power of 300 mW. In this case, the eigenvalues of the low-threshold solution are four real values and one pair of complex conjugates. As the real parts of all eigenvalues are negative, the low threshold solution is a stable focus or a fixed-point solution.

By inserting the corresponding high-threshold solution the same calculation yields a different set of eigenvalues, namely four real values and one pair of complex conjugates. However, one of the real eigenvalues is positive, which means that the high-threshold solution is a saddle point and thus unstable.

To obtain a broader overview on the divide-by-2 OPO stability, we have calculated the eigenvalues throughout the plane defined by the detunings Δ_e and Δ_o. We have found the eigenvalues of either one of the high- and the low-threshold solution to be symmetric for positive and negative detunings, i.e., the solution for a certain set of detunings (Δ_e,Δ_o) yields the same eigenvalues as the corresponding set of negative detunings $(-\Delta_e,-\Delta_o)$.

Figure 7 shows the different kinds of equilibria of the low-threshold solution, depicted by different gray tones as a function of the positive cavity detunings, which is equivalent to the case of negative detunings. For the whole locking area we find that the self-injection locking is stable. The case that was chosen in the example above ($\Delta_e=50$ MHz, $\Delta_o=45$ MHz) is depicted in Fig. 7 by the cross symbol.

When calculating the eigenvalues of the high-threshold solutions throughout the locking area, one finds that in most cases, the solution is an unstable saddle point. In the area of small detunings ($\Delta_e,\Delta_o<35$ MHz) and at the edges of the locking area, however, one can find single points, where the real parts of all eigenvalues are negative and where the solution thus is a stable solution. In this region, the absolute value of the real part of one eigenvalue is very small ($\approx10^{-16}$ as compared to the other eigenvalues), and small changes of

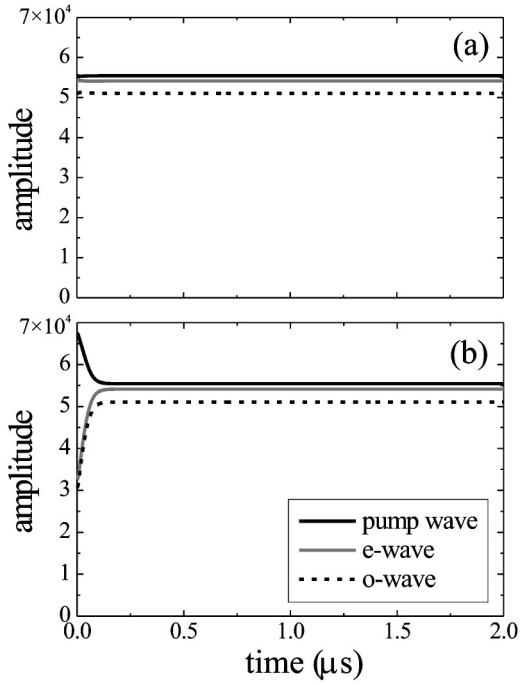

FIG. 8. Time evolution of the amplitudes of the OPO fields for a pump rate of 1.22×10^{13} Hz, a quarter-wave plate rotation angle of $\vartheta_{QWP}=6°$, and cavity detunings of $\Delta_e=32$ MHz and $\Delta_o=36$ MHz: the pump wave as solid black curve, the e-wave as solid gray curve, and the o-wave as dashed black curve. (a) Time evolution with the low-threshold steady-state values, and (b) with the high-threshold steady-state values as initial values for the numerical integration.

Δ_e, Δ_o, or f have a strong effect on the eigenvalue, causing frequent changes of the sign of the real part. As a result, the high-threshold solution changes from a stable to an unstable equilibrium upon minimal changes of the detunings or the pump rate.

In order to check the analytical results and also to yield unambiguous results for those detunings with one eigenvalue of the high-threshold solution close to zero, the nonlinear coupled field equations were numerically integrated for a number of cavity detunings Δ_e and Δ_o, as it was described in Sec. III C. A specific example with cavity detunings of $\Delta_e=32$ MHz and $\Delta_o=36$ MHz (which corresponds to a point yielding a stable high-threshold equilibrium) is shown in Fig. 8. The pump, the signal, and the idler amplitude are displayed as a function of time, once for the case that the coupled field equations are integrated with the low-threshold steady-state values as the initial values [Fig. 8(a)], and a second time with the high-threshold steady-state values inserted as initial values [Fig. 8(b)]. As one can see from Fig. 8(a), the amplitudes of the three OPO fields remain at their initial values, which demonstrates the stability of the low-threshold solution. In contrast, when starting the integration from the high-threshold solutions, the amplitudes quickly (within the cavity lifetime of 0.2 μs) leave the high-threshold values and attain the low-threshold values, in agreement with the prediction of the stability analysis. Also the phases of the three fields attain the steady-state values of the low-threshold solution (not shown).

For further numerical tests, the coupled field equations have been integrated for detunings throughout the entire locking area, which always, without a single exception, yielded the lower-threshold solution as the steady state. Also in the cases where, using the linear stability analysis, the high-threshold solution has been found to be stable, during the numerical evaluation the three OPO fields always assume the low-threshold steady-state values. From this we conclude, that despite the fact that the calculation of the eigenvalues yielded stable high-threshold solutions for few situations, the low-threshold solution for the triply-resonant divide-by-two OPO is the only stable solution of this system.

In the previous paragraphs, the dependence of the eigenvalues of the cavity detunings was discussed. However, as can be seen from Eqs. (A2), (A3), (A5), (A7), and (A10), the eigenvalues via the e- and the o-wave amplitudes also depend on the external pump rate f. As f is a parameter that can be changed in the course of an experiment, it should be studied, if the stable (low-threshold) branch is stable for any pump rate, or if there is a critical value of f, where a stability bifurcation occurs.

The eigenvalues of the low-threshold solution have been calculated in the described manner throughout the locking area for pump rates of up to 2.2×10^{16} Hz, corresponding to an external pump power of 1 MW. Note that an increased pump rate also results in an increased locking area, as it becomes possible to operate the OPO above threshold with larger detunings. Above a pump rate of about 2×10^{14} Hz, two areas evolve within the locking area, within which the low-threshold solutions are unstable. The unstable areas increase with increasing pump rate, continually covering a larger portion of the locking area. As an example, Fig. 9 shows the stable and unstable areas within the locking area for a pump rate of 2.2×10^{14} Hz. For each set of detunings Δ_e,Δ_o, there is a critical pump rate f_H, where a Hopf bifurcation occurs. At pump rates $>f_H$, the solution is a limit cycle. To demonstrate this behavior, the coupled field equations have been integrated for parameters that fall within the unstable area of Fig. 9(a) (see cross symbol). The result is shown in Fig. 9(b). The traces of the e- and the o-wave are displayed in a polar diagram, amplitudes as radius, and phases as angle. One can clearly see that both waves do not assume steady-state values, but keep oscillating around the solutions on limit cycles. We note that the pump wave (not shown) performs an analog oscillation around its steady-state solution.

The high-threshold solutions, on the other hand, remain unstable when increasing the pump rate. For pump rates up to 2.2×10^{16}, the behavior throughout the locking range is the same as was observed before.

In summary, the eigenvalues have been investigated as a function of the cavity detunings Δ_e and Δ_o spanning the range of 1.2×10^{13} to 2.2×10^{16} Hz. For low pump rates, the low-threshold solution for any set of detunings (Δ_e,Δ_o) was found to be always stable, while the high-threshold solution was found to be unstable. At a critical pump rate $f_H(\Delta_e,\Delta_o)$, a Hopf bifurcation occurs at the low-threshold branch, and the stable solution changes to a limit cycle solution for $f>f_H$.

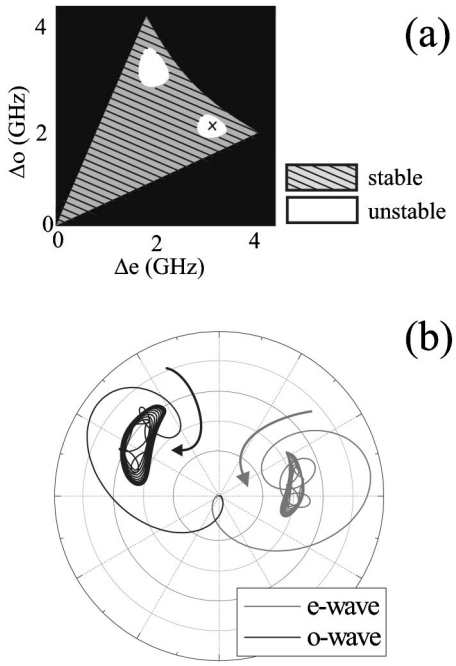

FIG. 9. (a) Stable and unstable low-threshold solutions found within the locking area at a pump rate of 2.2×10^{14} Hz. (b) Time evolution of the e-wave (gray curve) and the o-wave (black curve) displayed in a polar coordinate system with amplitude as radius, and phases as angle. Parameters for the calculation are $\Delta_e=3.1$ GHz, $\Delta_o=2.0$ GHz, $\vartheta_{QWP}=6°$, and $f=2.2\times10^{14}$ Hz [corresponding to location depicted by cross symbol in (a)].

B. Doubly resonant case

From a practical point of view, the stability of a doubly resonant OPO (DRO) is of some importance. Such a DRO could be realized by only enhancing the two subharmonic waves in a cavity, while the cavity is not resonant for the pump wave. The disadvantage of an enhanced threshold on one hand, a DRO could, on the other hand, provide easier handling due to the redundant electronic stabilization of the cavity length to the pump wavelength.

The DRO can be described by substituting the cavity internal pump field Eq. (1a) within the coupled field equations by a time independent traveling wave:

$$q_p = q_{in}, \tag{17a}$$

$$\frac{1}{2}(\kappa_e - i\Delta_e)q_e = iDq_o^*q_p + \gamma q_o, \tag{17b}$$

$$\frac{1}{2}(\kappa_o - i\Delta_o)q_o = iDq_pq_e^* - \gamma^* q_e. \tag{17c}$$

From Eqs. (17b) and (17c), one obtains the same locking condition Eq. (7) as for the triply resonant OPO. From Eqs. (17a)–(17c) a linearized system of six equations can be derived, analogous to the triply resonant case described above. However, due to Eq. (17a) not occurring in the interdependent system, the linear matrix reduces to a 4×4 matrix, the determinant of which satisfies

$$\begin{vmatrix} -\frac{1}{2}(\kappa_e - i\Delta_e) - \lambda & \gamma & 0 & iD\overline{q_p} \\ -\gamma^* & -\frac{1}{2}(\kappa_o - i\Delta_o) - \lambda & iD\overline{q_p} & 0 \\ 0 & -iD\overline{q_p^*} & -\frac{1}{2}(\kappa_e + i\Delta_e) - \lambda & \gamma^* \\ -iD\overline{q_p^*} & 0 & -\gamma & -\frac{1}{2}(\kappa_o + i\Delta_o) - \lambda \end{vmatrix} = 0. \quad (18)$$

The eigenvalues λ are solutions of the quartic characteristic equation

$$\lambda^4 + \xi_3\lambda^3 + \xi_2\lambda^2 + \xi_1\lambda + \xi_0 = 0, \quad (19)$$

where the coefficients ξ_i are all real. The explicit form of the coefficients is given in Appendix B.

In the DRO case, the eigenvalues depend only on the cavity loss parameters κ_e, κ_o, the cavity detunings Δ_e, Δ_o, and on the coupling parameter γ_0. Independent of the pump rate, the eigenvalues and therefore the stability of the system can be determined directly for a given set of external cavity parameters. The eigenvalues have been calculated for different coupling strengths and for different cavity detunings Δ_e and Δ_o, and as a result, the low-threshold solution is always found to be stable, while the high-threshold solution is always unstable.

In conclusion, a linear stability analysis of the triply resonant case as well as of the doubly resonant case has been carried out. It has been shown that the divide-by-2 OPO has only a single stable threshold equilibrium. Of the two equilibria with different pump power at threshold obtained by the analytical steady-state solution, only the lower-threshold equilibrium is stable, while the higher-threshold is an unstable equilibrium. At the low-threshold branch of the triply resonant OPO, a Hopf bifurcation occurs at a critical pump rate. Upon exceeding that pump rate, the stable low-threshold solutions turn into limit cycles, where the three OPO waves oscillate around the steady-state solutions.

VI. PHASE EIGENSTATES

As a result of the analytical investigations it was also found that, for each of the two threshold solutions, the OPO can assume one of two phase eigenstates. These two eigenstates have been found to be equivalent in their steady-state properties and stability, because the eigenvalues do not depend on absolute phase values, but only on the phase difference $(\varphi_e - \varphi_o - \theta)$ [see Eqs. (A5), (A7), and (A10)].

The numerical evaluation of the OPO field amplitudes and phases, however, offers the possibility to investigate the dynamics of individual phase eigenstates. In this section, we investigate how the assumed eigenstate depends on the initial values by numerically integrating the coupled field equations for various values of the OPO's external parameters.

As a result, we find that indeed either one of two different phase states appears as steady state value. As expected from the analytical calculations, none of the external parameters, but only the initial values of the subharmonic phases proved to have an influence on which of the two phase states is assumed in steady state.

In Fig. 10, two examples are shown that demonstrate the influence of the initial phase. In both cases, the self-injection term is "switched on" after 0.5 μs, to make the effect of self-injection visible. Both numerical integrations are performed with the same external parameters, in particular the same cavity detunings of $\Delta_e = 30$ MHz and $\Delta_o = 69$ MHz and the same initial conditions (absolute values of the subharmonic fields). Only different initial phases φ_e and φ_o are used, namely $\varphi_e^0 = -0.7$ and $\varphi_o^0 = 0.7$ for the upper graph [10(a)] and $\varphi_e^0 = -0.8$ and $\varphi_o^0 = 0.8$ for the lower graph [10(b)]. This variation results in the phases assuming different steady-state values that are separated by π. We note that the different phase states assumed have no influence on the absolute values of amplitudes, i.e., on the output power on the subharmonic waves.

For a full overview on the phase development towards steady state, the integration was repeated as described; however, the initial phases φ_e and φ_o were both varied in equi-

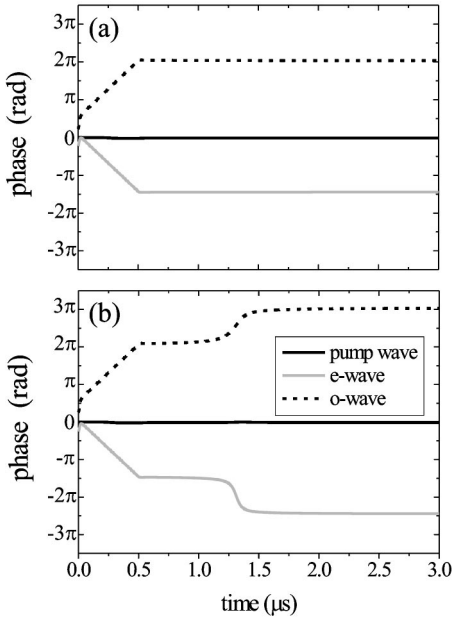

FIG. 10. Time evolution of the phases of the OPO fields for a pump rate of $f = 1.22 \times 10^{13}$ Hz, a quarter-wave plate rotation angle of $\vartheta_{QWP} = 6°$, and cavity detunings of $\Delta_e = 30$ MHz and $\Delta_o = 69$ MHz: the pump wave as solid black curve, the e-wave as solid gray curve, and the o-wave as dashed black curve. (a) With initial phases of $\varphi_e^0 = -0.7$ and $\varphi_o^0 = 0.7$, the phases of the coupled field equations assume steady-state values $\overline{\varphi_{e,1}} = -4.53$ and $\overline{\varphi_{o,1}} = 6.38$, and (b) with the same parameters, but with changed initial phases of $\varphi_e^0 = -0.8$ and $\varphi_o^0 = 0.8$ the phases assume steady-state values $\overline{\varphi_{e,2}} = -7.67 = \overline{\varphi_{e,1}} - \pi$ and $\overline{\varphi_{o,2}} = 9.52 = \overline{\varphi_{o,1}} + \pi$.

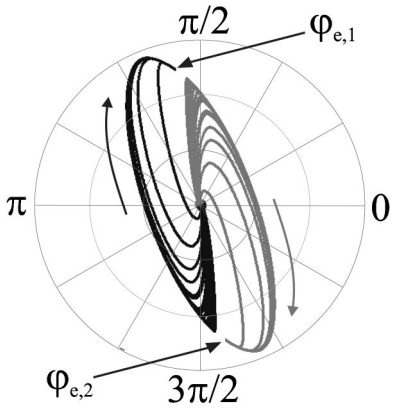

FIG. 11. Traces of the e-wave for different initial values of the phase difference $\varphi_e - \varphi_o$ with amplitudes as radius and phases as angle using polar coordinates. Traces ending in the first phase state are plotted black; traces assuming the second phase state are gray. Parameters for the calculation are $f = 1.22 \times 10^{13}$ Hz, $\vartheta_{QWP} = 6°$, $\Delta_e = 30$ MHz, and $\Delta_o = 69$ MHz

distant steps of $2\pi/100$. The calculations have been carried out for a pump rate of $f = 1.22 \times 10^{13}$ Hz, a quarter-wave plate rotation angle of $\vartheta_{QWP} = 6°$ and cavity detunings $\Delta_e = 30$ MHz and $\Delta_o = 69$ MHz. The result is shown in Fig. 11, where only the traces of the e-wave are plotted using polar coordinates, i.e., the amplitude b_e as radius and the phase φ_e as angle. Traces which end in the first phase state $\varphi_{e,1} = 1.75$ are plotted on black, those assuming the second state $\varphi_{e,2} = 6.38$ are gray. In Fig. 11, one can see that all of the traces assume either one or the other of the two steady states, thereby dividing the (6-dimensional) phase space into a black and a gray region, i.e., into two perfectly symmetric basins of attraction. This clearly proves the twofold symmetry we were expecting to see.

From Fig. 11, one can also see that the traces describe a wide, curved arc, ending in the respective phase eigenstate, and that there is a strong preference for clockwise rotation of the traces in phase space. We found that this direction of rotation occurs only with asymmetric cavity detunings, and if $\Delta_e < \Delta_o$. When we chose the cavity detunings as equal, the phase states were assumed on a direct path, while with $\Delta_e > \Delta_o$, the traces performed a counterclockwise rotation before reaching steady state.

Regarding our numerical studies of stability of the divide-by-two OPO, we note that we did not observe any hopping between the two-phase eigenstates. Even the application of external disturbances (like a stepwise variation of the pump phase) led only to strongly damped relaxation oscillations of the three fields around the steady-state values. We noticed that a change of the cavity detuning (as would be caused by changing the cavity length) caused the steady-state values to relocate in phase space; however, the OPO fields quickly followed that relocation while remaining self-phase-locked.

In conclusion, from the described investigations it is evident that the phase state assumed by a self-phase-locked divider solely depends on the initial phases of the subharmonic waves. The two phase eigenstates are two equivalent attractors of the nonlinear system, dividing the phase-space into two symmetric basins of attraction. Upon applying disturbances not exceeding the cavity lifetime (i.e., within the validity of the slowly varying envelope approximation), we could observe that the OPO fields remain locked and follow the relocating steady-state solutions. This behavior is evidence of the OPO divider's high stability and its large locking range of several tens of MHz.

VII. SUMMARY

Phase-coherent division of an optical frequency by 2 based on a self-phase-locked cw OPO is investigated theoretically. By analytically solving the coupled field equations in steady state, the condition for occurrence of self-phase locking is derived. The dependence of the steady-state amplitudes and phases of the OPO fields is studied as a function of the detuning of the cavity modes from the subharmonic light field, the pump rate, and the quarter-wave plate rotation angle, with values being typical for a corresponding experiment.

Previously it has been shown that in the self-phase-locked case there are two formal steady-state solutions of the coupled field equations, which correspond to two different values for the OPO pump power at threshold. Our stability analysis, however, applied to these solutions for the triply resonant as well as the doubly resonant OPO, shows that only the solution corresponding to the lower threshold state is stable. The higher threshold solutions are unstable, which is in contrast to previous expectations. The stability analysis is completed by numerical integration of the coupled field equations, which for any set of parameters leads only to a single, stable threshold state, which is that of the lower threshold.

Furthermore, the analytical solution reveals the existence of two phase-eigenstates, which show to be equivalent and indistinguishable in steady state. Via numerical integration of the coupled field equations that allow also a study of the temporal development of any initial state off equilibrium, we find that self-phase-locked divide-by-2 OPOs indeed possess two sets of phase eigenstates, which are separated from each other by π. The initial phases of the two subharmonic fields determine which eigenstate is assumed, independent of any experimental parameter. The two phase eigenstates form two equivalent attractors of the nonlinear system, dividing phase space into two symmetric basins of attraction.

In conclusion, we have presented a comprehensive theoretical description of the self-phase-locked divide-by-2 OPO that significantly improves the physical understanding of self-phase-locked OPOs employed as all-optical frequency divider. The present work may thus be helpful for further improvement in design and operation of dividers to aid high-precision metrology in the mid and far infrared.

ACKNOWLEDGMENTS

The authors acknowledge financial support by the Dutch Stichting Voor Fundamenteel Onderzoek der Materie (FOM). We are grateful to Dr. J.-J. Zondy for fruitful discussions on the linear stability analysis and to Dr. H. L. Offerhaus for

continuous discussions on the working principle of frequency dividers.

APPENDIX A: THE COEFFICIENTS OF THE CHARACTERISTIC EQUATION: TRO CASE

In the following, the coefficients ξ_5 to ξ_0 of the characteristic Eq. (16) are derived from the determinant of Eq. (15).

The coefficients ξ_5, ξ_4 and ξ_3 are easily found to be real:

$$\xi_5 = \kappa_p + \kappa_e + \kappa_o, \tag{A1}$$

$$\xi_4 = \frac{1}{4}(\kappa_p^2 + \kappa_e^2 + \kappa_o^2 + \Delta_e^2 + \Delta_o^2) + \kappa_p\kappa_e + \kappa_p\kappa_o + \kappa_e\kappa_o - 2D^2(b_p^2 - b_e^2 - b_o^2) + 2\gamma_0^2, \tag{A2}$$

$$\xi_3 = (\gamma_0^2 - D^2 b_p^2)(2\kappa_p + \kappa_e + \kappa_o) + D^2 b_e^2(\kappa_p + 2\kappa_e + \kappa_o) + D^2 b_o^2(\kappa_p + \kappa_e + 2\kappa_o) + \frac{1}{4}(\kappa_e^2 + \Delta_e^2)(\kappa_p + \kappa_o) + \frac{1}{4}(\kappa_o^2 + \Delta_o^2)(\kappa_p + \kappa_e) + \frac{1}{4}\kappa_p^2(\kappa_e + \kappa_o) + \kappa_p\kappa_e\kappa_o. \tag{A3}$$

The coefficient ξ_2 includes four imaginary terms, which are two pairs of complex conjugate terms and can be summarized, such that one yields a purely real expression as it is described in the following:

$$\begin{aligned} &iD^2\Delta_e\gamma q_e^* q_o - iD^2\Delta_e\gamma^* q_e q_o^* + iD^2\Delta_o\gamma q_e^* q_o - iD^2\Delta_o\gamma^* q_e q_o^* \\ &= D^2(\Delta_e + \Delta_o)(i\gamma q_e^* q_o - i\gamma^* q_e q_o^*) \\ &= D^2(\Delta_e + \Delta_o)\gamma_0 b_e b_o (ie^{i(\theta+\varphi_o-\varphi_e)} + \text{c.c.}) \\ &= 2D^2(\Delta_e + \Delta_o)\gamma_0 b_e b_o \sin(\varphi_e - \varphi_o - \theta). \end{aligned} \tag{A4}$$

With the imaginary parts summarized as shown in expression (A4), the real coefficient ξ_2 reads as follows:

$$\begin{aligned} \xi_2 = {} & D^4(b_e^2 + b_o^2 - b_p^2)^2 + 2D^2\gamma_0^2(b_e^2 + b_o^2 - b_p^2) + \gamma_0^2\left(\gamma_0^2 + \frac{1}{2}\kappa_p^2 + \kappa_p\kappa_e + \kappa_p\kappa_o + \frac{1}{2}\kappa_e\kappa_o - \frac{1}{2}\Delta_e\Delta_o\right) \\ & - D^2 b_p^2\left(\frac{1}{2}\kappa_p^2 + \kappa_p\kappa_e + \kappa_p\kappa_o + \frac{1}{2}\kappa_e\kappa_o + \frac{1}{2}\Delta_e\Delta_o\right) + D^2 b_e^2\left(\frac{1}{2}\kappa_e^2 + \frac{1}{2}\Delta_e^2 + \kappa_p\kappa_e + \kappa_e\kappa_o + \frac{1}{2}\kappa_p\kappa_o\right) \\ & + D^2 b_o^2\left(\frac{1}{2}\kappa_o^2 + \frac{1}{2}\Delta_o^2 + \kappa_p\kappa_o + \kappa_e\kappa_o + \frac{1}{2}\kappa_p\kappa_e\right) + \frac{1}{4}\kappa_p\kappa_e\kappa_o(\kappa_p + \kappa_e + \kappa_o) + \frac{1}{16}(\kappa_e^2 + \Delta_e^2)(\kappa_o^2 + \Delta_o^2) + \frac{1}{16}\kappa_p^2(\kappa_e^2 + \kappa_o^2 + \Delta_e^2 + \Delta_o^2) \\ & + \frac{1}{4}\kappa_p\kappa_e\Delta_o^2 + \frac{1}{4}\kappa_p\Delta_e^2\kappa_o + 2D^2(\Delta_e + \Delta_o)\gamma_0 b_e b_o \sin(\varphi_e - \varphi_o - \theta). \end{aligned} \tag{A5}$$

Calculating the coefficient ξ_1, one finds eight complex terms, which are four pairs of complex conjugate numbers and can be rewritten and summarized analogously:

$$\begin{aligned} &\frac{1}{2}iD^2\kappa_p\Delta_o\gamma q_e^* q_o - \frac{1}{2}iD^2\kappa_p\Delta_o\gamma^* q_e q_o^* + \frac{1}{2}iD^2\kappa_p\Delta_e\gamma q_e^* q_o - \frac{1}{2}iD^2\kappa_p\Delta_e\gamma^* q_e q_o^* + \frac{1}{2}iD^2\kappa_e\Delta_o\gamma q_e^* q_o - \frac{1}{2}iD^2\kappa_e\Delta_o\gamma^* q_e q_o^* \\ &+ \frac{1}{2}iD^2\kappa_o\Delta_e\gamma q_e^* q_o - \frac{1}{2}iD^2\kappa_o\Delta_e\gamma^* q_e q_o^* = \frac{1}{2}D^2[\Delta_e(\kappa_p + \kappa_o) + \Delta_o(\kappa_p + \kappa_e)](i\gamma q_e^* q_o + \text{c.c.}) \\ &= D^2\gamma_0 b_e b_o \sin(\varphi_e - \varphi_o - \theta)[\Delta_e(\kappa_p + \kappa_o) + \Delta_o(\kappa_p + \kappa_e)]. \end{aligned} \tag{A6}$$

The real coefficient ξ_1 is then given by

$$\begin{aligned} \xi_1 = {} & D^4(b_p^2\kappa_p - b_e^2\kappa_e - b_o^2\kappa_o)(b_p^2 - b_e^2 - b_o^2) - D^2 b_p^2\left[2\gamma_0^2\kappa_p + \frac{1}{2}\kappa_p\Delta_e\Delta_o + \frac{1}{4}\kappa_p^2(\kappa_e + \kappa_o)\right] \\ & + D^2 b_e^2\left[\gamma_0^2(\kappa_p + \kappa_e) + \frac{1}{4}(\kappa_p + \kappa_o)(\kappa_e^2 + \Delta_e^2)\right] + D^2 b_o^2\left[\gamma_0^2(\kappa_p + \kappa_o) + \frac{1}{4}(\kappa_p + \kappa_e)(\kappa_o^2 + \Delta_o^2)\right] \\ & + \gamma_0^2\left[\gamma_0^2\kappa_p + \frac{1}{4}\kappa_p^2(\kappa_e + \kappa_o) - \frac{1}{2}\kappa_p\Delta_e\Delta_o\right] + \frac{1}{2}\kappa_p\kappa_e\kappa_o[\gamma_0^2 + D^2(b_e^2 + b_o^2 - b_p^2)] + \frac{1}{16}\kappa_p^2\kappa_e\kappa_o(\kappa_e + \kappa_o) + \frac{1}{16}\kappa_p^2(\kappa_e\Delta_o^2 + \Delta_e^2\kappa_o) \\ & + \frac{1}{16}\kappa_p(\Delta_e^2 + \kappa_e^2)(\Delta_o^2 + \kappa_o^2) + D^2\gamma_0 b_e b_o \sin(\varphi_e - \varphi_o - \theta)[\Delta_e(\kappa_p + \kappa_o) + \Delta_o(\kappa_p + \kappa_e)]. \end{aligned} \tag{A7}$$

The last coefficient contains eight complex terms, which can be rewritten analogously,

$$iD^4b_o^2\Delta_o\gamma q_e^* q_o - iD^4b_o^2\Delta_o\gamma^* q_e q_o^* + iD^4b_e^2\Delta_e\gamma q_e^* q_o - iD^4b_e^2\Delta_e\gamma^* q_e q_o^* + i\frac{1}{4}D^2\kappa_p\kappa_e\Delta_o\gamma q_e^* q_o - i\frac{1}{4}D^2\kappa_p\kappa_e\Delta_o\gamma^* q_e q_o^*$$
$$+ i\frac{1}{4}D^2\kappa_p\Delta_e\kappa_o\gamma q_e^* q_o - i\frac{1}{4}D^2\kappa_p\Delta_e\kappa_o\gamma^* q_e q_o^*$$
$$= \left[2D^4(b_o^2\Delta_o + b_e^2\Delta_e) + \frac{1}{2}D^2\kappa_p(\kappa_e\Delta_o + \Delta_e\kappa_o)\right]\gamma_o b_e b_o \sin(\varphi_e - \varphi_o - \theta) \tag{A8}$$

and in addition one finds two terms which contain the quadratic complex steady state values:

$$-D^4\gamma^2 q_e^{*2} q_o{}^2 - D^4\gamma^{*2} q_e{}^2 q_o^{*2} = -D^4\gamma_0^2 b_e^2 b_o^2 (e^{i(2\varphi_e - 2\varphi_o - 2\theta)} + \text{c.c.})$$
$$= -2D^4\gamma_0^2 b_e^2 b_o^2 \cos(2\varphi_e - 2\varphi_o - 2\theta)$$
$$= -2D^4\gamma_0^2 b_e^2 b_o^2 [1 - 2\sin^2(\varphi_e - \varphi_o - \theta)]. \tag{A9}$$

With these two real terms, the real coefficient ξ_0 can be written as follows:

$$\xi_0 = -4D^6 b_p^2 b_e^2 b_o^2 + 2D^4\gamma_0^2 b_e^2 b_o^2 + \frac{1}{4}D^4[b_p^4\kappa_p^2 + b_e^4(\kappa_e^2 + \Delta_e^2) + b_o^4(\kappa_o^2 + \Delta_o^2)] + \frac{1}{2}D^4 b_e^2 b_o^2(\kappa_e\kappa_o + \Delta_e\Delta_o) - \frac{1}{2}D^4(b_p^2 b_e^2\kappa_p\kappa_e + b_p^2 b_o^2\kappa_p\kappa_o)$$
$$- D^2 b_p^2\left(\frac{1}{8}\kappa_p^2\kappa_e\kappa_o + \frac{1}{8}\kappa_p^2\Delta_e\Delta_o + \frac{1}{2}\gamma_0^2\kappa_p^2\right) + D^2 b_e^2\left(\frac{1}{2}\gamma_0^2\kappa_p\kappa_e + \frac{1}{8}\kappa_p\Delta_e^2\kappa_o + \frac{1}{8}\kappa_p\kappa_e^2\kappa_o\right)$$
$$+ D^2 b_o^2\left(\frac{1}{2}\gamma_0^2\kappa_p\kappa_o + \frac{1}{8}\kappa_p\kappa_e\Delta_o^2 + \frac{1}{8}\kappa_p\kappa_e\kappa_o^2\right) + \gamma_0^2\kappa_p^2\left(\frac{1}{4}\gamma_0^2 + \frac{1}{8}\kappa_e\kappa_o - \frac{1}{8}\Delta_e\Delta_o\right) + \frac{1}{64}\kappa_p^2(\kappa_e^2 + \Delta_e^2)(\kappa_o^2 + \Delta_o^2)$$
$$+ \gamma_o b_e b_o \sin(\varphi_e - \varphi_o - \theta)\left[2D^4(b_o^2\Delta_o + b_e^2\Delta_e) + \frac{1}{2}D^2\kappa_p(\kappa_e\Delta_o + \Delta_e\kappa_o)\right] - 2D^4\gamma_0^2 b_e^2 b_o^2[1 - 2\sin^2(\varphi_e - \varphi_o - \theta)]. \tag{A10}$$

APPENDIX B: THE COEFFICIENTS OF THE CHARACTERISTIC EQUATION: DRO CASE

In this paragraph, the coefficients ξ_3 to ξ_0 of the characteristic Eq. (19) of the doubly resonant OPO are given:

$$\xi_3 = \kappa_e + \kappa_o, \tag{B1a}$$

$$\xi_2 = \kappa_e\kappa_o + \frac{1}{4}\kappa_e^2 + \frac{1}{4}\kappa_o^2 + \frac{1}{4}\Delta_e^2 + \frac{1}{4}\Delta_o^2 - 2(D^2 b_p^2 - \gamma_0^2), \tag{B1b}$$

$$\xi_1 = \frac{1}{4}\Delta_e^2\kappa_o + \frac{1}{4}\Delta_o^2\kappa_e + \frac{1}{4}\kappa_e^2\kappa_o + \frac{1}{4}\kappa_o^2\kappa_e - (\kappa_e + \kappa_o)(D^2 b_p^2 - \gamma_0^2), \tag{B1c}$$

$$\xi_0 = \frac{1}{16}\Delta_e^2\Delta_o^2 + \frac{1}{16}\kappa_e^2\kappa_o^2 + \frac{1}{16}\Delta_e^2\kappa_o^2 + \frac{1}{16}\Delta_o^2\kappa_e^2 + (D^2 b_p^2 - \gamma_o^2)^2 - \frac{1}{2}\kappa_e\kappa_o(D^2 b_p^2 - \gamma^2) - \frac{1}{2}\Delta_e\Delta_o(D^2 b_p^2 - \gamma^2) - \Delta_e\Delta_o\gamma_0^2. \tag{B1d}$$

After inserting the pump wave amplitude given by Eq. (8), the eigenvalues can be simplified to read

$$\xi_3 = \kappa_e + \kappa_o, \tag{B2a}$$

$$\xi_2 = \left(\frac{1}{2}\kappa_e + \frac{1}{2}\kappa_o\right)^2 + \left(\frac{1}{2}\Delta_e - \frac{1}{2}\Delta_o\right)^2 \mp 2\sqrt{\alpha}, \tag{B2b}$$

$$\xi_1 = (\Delta_e - \Delta_o)\left(\frac{1}{4}\Delta_e\kappa_o - \frac{1}{4}\Delta_o\kappa_e\right) \mp (\kappa_o + \kappa_e)\sqrt{\alpha}, \tag{B2c}$$

$$\xi_0 = 15\gamma_0^2\Delta_e\Delta_o - \frac{15}{16}(\Delta_e\kappa_o - \Delta_o\kappa_e)^2. \tag{B2d}$$

In the above Eqs. (B2a)–(B2d), the upper sign of $\mp$ belongs to the high-threshold solution, whereas the lower one belongs to the low-threshold solution, with α being defined as in Eq. (6).

[1] Th. Becker *et al.*, Phys. Rev. A **63**, 051802 (2001).
[2] J. Reichert, R. Holzwarth, Th. Udem, and T. W. Hänsch, Opt. Commun. **172**, 59 (1999).
[3] D.-H. Lee, M. E. Klein, J.-P. Meyn, R. Wallensten, P. Groß, and K.-J. Boller, Phys. Rev. A **67**, 013808 (2003).
[4] Y. Kobayashi and K. Torizuka, Opt. Lett. **25**, 856 (2000).
[5] E. J. Mason and N. C. Wong, Opt. Lett. **23**, 1733 (1998).
[6] H. H. Adamyan and G. Yu. Kryuchkyan, Phys. Rev. A **69**, 053814 (2004).
[7] C. Fabre, E. J. Mason, and N. C. Wong, Opt. Commun. **170**, 299 (1999).
[8] P. Groß, K.-J. Boller, M. E. Klein, and D.-H. Lee, *Conference on Lasers and Electro-Optics*, postdeadline papers book (Optical Society of America, Washington, DC, 2003), postdeadline paper no. CPDB1.
[9] P. Groß, M. E. Klein, and K.-J. Boller, *Conference on Lasers and Electro-Optics*, OSA Technical Digest CD-ROM, postconference edition (Optical Society of America, Washington, DC, 2004), paper no. CMH2.
[10] A. E. Siegman, *Laser Injection Locking* (University Science Books, Mill Valley, CA, 1986), Chap. 29, pp. 1130–1170.
[11] W. Brunner and H. Paul, Opt. Commun. **19**, 253 (1976).
[12] D.-H. Lee *et al.*, Proc. SPIE **3928**, 25 (2000).
[13] A. L. Garcia, *Numerical Methods for Physics*, 2nd ed. (Prentice Hall, Inc., Upper Saddle River, NJ, 2000), Chap. 3, pp. 67–105, ISBN 0-13-906744-2.
[14] R. Graham and H. Haken, Z. Phys. **210**, 276 (1968).
[15] D.-H. Lee, M. E. Klein, and K.-J. Boller, Appl. Phys. B: Lasers Opt. **66**, 747 (1998).
[16] K. P. Chung and A. Marcano O., J. Opt. Soc. Am. B **5**, 2524 (1988).
[17] J.-J. Zondy, A. Douillet, A. Tallet, E. Ressayre, and M. Le Berre, Phys. Rev. A **63**, 023814 (2001).
[18] J.-J. Zondy, Phys. Rev. A **67**, 035801 (2003).
[19] I. D. Huntley and R. M. Johnson, *Linear and Nonlinear Differential Equations*, Ellis Horwood Series in Mathematics and its Applications (Ellis Horwood Limited, Chichester, 1983).
[20] M. Vidyasagar, *Nonlinear Systems Analysis*, 2nd ed. (Prentice Hall, Englewood Cliffs, NJ, 1993).